# Scaling properties of a class of shell models

P. Frick,[1,2] B. Dubrulle,[3,4] and A. Babiano[1]
[1]*LMD, Ecole Normale Supérieure, 24 rue Lhomond, F-75005 Paris, France*
[2]*Institute of Continuous Media Mechanics, Korolyov 1, 614061 Perm, Russia*
[3]*Centre National de la Recherche Scientifique, UPR 182, Service d'Astrophysique, Centre d'Etudes Nucléaires de Saclay, L'Orme des Merisiers, Bâtiment 709, F-91191 Gif sur Yvette, France*
[4]*Centre National de la Recherche Scientifique, URA 285, Observatoire Midi-Pyrénées, 14 avenue Belin, F-31400 Toulouse, France*
(Received 10 May 1994; revised manuscript received 10 November 1994)

The scaling properties of a class of shell models are studied, via their velocity structure functions. The models all conserve energy and the fundamental symmetries of the Navier-Stokes equations. They also conserve a second quantity, which depends on the coefficients of the nonlinear terms, parametrized by $\varepsilon$. Models with $\varepsilon$ varying from 0.2 to 10 are considered. All the models are found to display extended self-similarity, which allows a better estimate of the scaling exponents of the structure functions at any order. In most cases, deviations from Kolmogorov 1941 scaling are observed. As in fully developed turbulence, this intermittency is consistent with probability distribution functions resembling logarithmic Poisson distributions (exponential wings, negative skewness). Their signature is a hierarchical structure of the moments of the energy dissipation. The hierarchy is characterized by two main parameters, $\Delta$ and $\beta$, describing, respectively, the smallest dissipative scales and the degree of intermittency of the energy transfers. These parameters are measured in each shell model and the curves $\Delta$ and $\beta$ as a function of $\varepsilon$ are obtained. Two interesting transitions are obtained, for $\varepsilon=0.39$ and $\varepsilon=1$. In the first case, the system goes from nonintermittent to intermittent, with $\beta$ and $\Delta$ going from $\beta=1$, $\Delta=0$ to $\beta<1$, $\Delta\neq 0$. This transition corresponds to the stable-unstable transition in some mapping characterizing the shell models. In the second case, discontinuities in both $\beta$ and $\Delta$ are observed. This transition corresponds to the separation between models with "helicitylike" or "enstrophylike" conservation laws. Apart from these interesting transitions, no obvious correlation between the three parameters is found, indicating the complexity of the scaling character. Shell models, however, stand as a powerful tool to investigate the scale invariance, and the development of a complete theory which may help in understanding fully developed turbulence.

PACS number(s): 47.27.Gs, 47.27.Eq

## I. INTRODUCTION

Among the various symmetries satisfied by the Navier-Stokes equation, the scale invariance is the most appealing and the most mysterious. Its existence suggests the possibility of a universal description of the turbulence. Yet, even in the simple isotropic case, the evidence of universality is not compelling. In two-dimensional flows, the shape of the energy spectrum appears to depend critically on the nature of the coherent vortices generated by the interplay between energy input and dissipation [1,2]. In three dimensions, this dependence is milder and seems more connected with the spatial distribution of the dissipative structures. Higher order statistical indicators do not follow the prediction obtained within the framework of local scale invariance. For example, the exponents of the structure functions of the velocity increments over a small distance $l$ do not follow the linear $\zeta_p=p/3$ law predicted by Kolmogorov.

New perspectives were offered recently by a model of intermittency proposed by She and Lévêque [3]. This model relies on a hierarchical structure of the moments of energy dissipation. It is characterized by only two parameters, $\Delta$ and $\beta$, characterizing, respectively, the geometry of the smallest dissipative scales and the degree of intermittency of the interactions [4]. The hierarchy was later shown to be related to a logarithmic Poisson statistics for the energy dissipation [4,5]. An interesting feature of the logarithmic Poisson distribution is its covariance with respect to a generalized scale transformation [4]. This led Dubrulle [4] to postulate that the hierarchy of the moments of energy dissipation could be directly related to the scale invariance property of the Navier-Stokes equation, and could then be a generic feature of a scale invariant system. It is then natural to investigate whether the moments hierarchy proposed by She and Lévêque also holds in simple representations of the Navier-Stokes equations, the shell models of turbulence. These models, described in Sec. II, are easier to study than the full nonlinear Navier-Stokes equations and present some analogy with incompressible fluid models. For example, they have quadratic nonlinearities and conserve energy. They can also be characterized by the conservation of an additional quantity, similar to a generalized enstrophy or helicity [6,7] which is equivalent to the helicity or the enstrophy only for specific values of the parameters describing the models [7]. In this sense, the shell models can be seen as simple generalizations of

 

two-dimensional (2D) or 3D turbulence. This raises another interesting issue, within the intermittency model of She and Lévêque: will the potential moment hierarchy also be characterized by the same parameters $\Delta=\beta=\frac{2}{3}$ [3] as in 3D isotropic turbulence? If the hierarchy is indeed directly connected with the scale invariance of the interactions, we may expect $\Delta$ and $\beta$ to be nonuniversal and dependent on the conservation laws or boundary conditions of the system [4]. The scale invariance symmetry would then enforce the shape of the interactions (the existence of the hierarchy) but not the value of the constants.

The goal of the present contribution is to explore partially this issue. Specifically, we shall examine whether the moment hierarchy observed in 3D isotropic turbulence [8] is also found in the generalized shell models, and study the variation of the corresponding parameters $\Delta$ and $\beta$ with the nature of the conservation laws (Sec. III).

## II. MAIN PROPERTIES OF THE GENERALIZED SHELL MODEL

### A. Description

The shell models were introduced in the 1970s [9,11] as an attempt to mimic the Navier-Stokes equations via dynamical systems with limited degrees of freedom. They are constructed by truncations of the Navier-Stokes equations in the Fourier space, retaining only one real or complex mode $U_n$ as a representative of all the modes in the shell of wave number $k$ between $k_n=k_0\lambda^n$ and $k_{n+1}$. The parameter $\lambda$ characterizes the ratio between two adjacent scales. It is one of the main parameters of the model, and is usually taken equal to $\lambda=2$. From now on, we shall adopt this value. Note, however, that other values may be considered [7]. The coupling between the shells is chosen so as to preserve the main symmetries and properties of the Navier-Stokes equations. In this paper, we shall consider a class of so-called GOY shell models (Gledzer, Ohkitani, and Yamada) in the form introduced in [6], which is governed by the following set of complex ordinary differential equations:

$$(d_t+\nu k_n^2)U_n=ik_n\left[U_{n+1}^*U_{n+2}^*-\frac{\varepsilon}{2}U_{n-1}^*U_{n+1}^*-\frac{(1-\varepsilon)}{4}U_{n-2}^*U_{n-1}^*\right]+f_n\ . \tag{1}$$

Here, the asterisk stands for the conjugate, $f_n$ is a random force, acting only on the few shells near $n=0$, and $\varepsilon$ is a free parameter. One gets the model of Gledzer [11] if $\varepsilon=1.25$ and the model of Yamada and Ohkitani [10] if $\varepsilon=0.5$.

In fully developed turbulence, an important dynamical quantity is the spectral flux of energy. The corresponding quantity in shell models, the flux of energy $\Pi_n$ from shells with $k<k_n$ to shells with $k\geq k_n$, can be written

$$\Pi_n=\left\langle \mathrm{Im}\left[k_nU_nU_{n-1}\left[-\frac{1}{2}U_{n+1}+\frac{\varepsilon-1}{4}U_{n-2}\right]\right]\right\rangle =k_n\left[\frac{\varepsilon-1}{4}\Theta_{n-1}-\frac{1}{2}\Theta_n\right], \tag{2}$$

where $\Theta_n=\langle\rho_{n-1}\rho_n\rho_{n+1}\sin(\phi_{n-1}+\phi_n+\phi_{n+1})\rangle$ and $U_n=\rho_ne^{i\phi_n}$.

### B. Properties

All the models in the GOY class are scale invariant in the inviscid, force-free limit ($f_n,\nu\to0$). Specifically, Eqs. (1) are formally invariant under the entire group of scaling transformations $\mathcal{D}_h$:

$$k_n\to\lambda^{-1}k_n,\quad U_n\to\lambda^hU_n,\quad t\to\lambda^{1-h}t,\quad \lambda>0 \tag{3}$$

with arbitrary similarity exponent $h$. This symmetry is also found in Navier-Stokes equations.

The GOY class of shell models is also characterized by a number of conservation laws, in the inviscid, force-free limit. The conserved quantity $W$ can be written

$$W=\sum_n|U_n|^2z^n\ , \tag{4}$$

where $z$ satisfies the quadratic equation [7]

$$(\varepsilon-1)z^2-\varepsilon z+1=0\ . \tag{5}$$

This equation admits two solutions, $z=1$ and $z=1/(\varepsilon-1)$. The first solution corresponds to the energy conservation

$$E=\sum_n|U_n|^2\ . \tag{6}$$

It is a conserved quantity common to all shell models. The second solution corresponds to the conservation of a generalized enstrophy:

$$H=\sum_n[\mathrm{sgn}(\varepsilon-1)]^nk_n^{\alpha(\varepsilon)}|U_n|^2\ , \tag{7}$$

where $\alpha(\varepsilon)=-\log_2(|\varepsilon-1|/2)$ and $\mathrm{sgn}(\varepsilon-1)=-1$ if $\varepsilon<1$ and $\mathrm{sgn}(\varepsilon-1)=1$ if $\varepsilon>1$. In the first case, the conserved quantity is similar to a "helicity" [7]; in the second case, it is more similar to an enstrophy.

The conserved quantities correspond to two sets of static solutions: Kolmogorov-like [$U_n=k_n^{-1/3}g_1(n)$, $g_1(n)$ being any periodic function of period 3] and fluxless-like ($U_n=k_n^{\gamma(\varepsilon)}g_2(n)$, $g_2(n)$ being any periodic function of period three, $\gamma=[\log_2(|\varepsilon-1|/2)]/3$), characterized by a negligible energy transfer ($\Pi_n=0$) [6]. The Kolmogorov solution corresponds to an ultraviolet stable fixed point of the ratio mapping $U_{n+3}/U_n$ for $0<\varepsilon<2$ and infrared stable fixed point otherwise. The stability of the second solution is opposite. Here, ultraviolet (infrared) stable means that the fixed point is asymptotically approached by forward (backward) iteration of the ratio map, corresponding to a cascade of energy from small (large) to large (small) scales. A numerical study of the transition to chaos in the shell models with $0<\varepsilon<1$ was

performed by Biferale *et al.* [6]. They found that the Kolmogorov static solution corresponds to a stable fixed point for $\varepsilon<\varepsilon_1=0.3843$. The point becomes unstable at $\varepsilon=\varepsilon_1$, via a Hopf bifurcation. For larger values of $\varepsilon$, the systems evolve into a chaotic state, following the Ruelle-Takens scenario. For $1>\varepsilon>\varepsilon_2=0.3953$, the dynamical evolution is intermittent with a positive Lyapunov exponent. This regime is characterized by a strange attractor remaining close to the Kolmogorov unstable fixed point.

The equivalent analysis for $\varepsilon>1$ has not been performed yet. It is complicated by the existence of backwards energy transfers induced by the conservation of the generalized enstrophy [15].

We may note several interesting cases.

(1) $\varepsilon=\frac{1}{2}$; in that case $\alpha=1$ and $\mathrm{sgn}(\varepsilon-1)=-1$: The two conserved quantities are the energy and the helicity [7]. This is the usual GOY model, which is considered as the analog of the isotropic 3D turbulence. It has been studied intensively both numerically [12,13,10] and analytically [14], using a closure model.

(2) $\varepsilon=1$; in that case $\alpha=\infty$, no cascade is possible.

(3) $\varepsilon=\frac{5}{4}$; in that case $\alpha=2$ and $\mathrm{sgn}(\varepsilon-1)=1$: The two conserved quantities are the energy and the enstrophy, as in two-dimensional turbulence. The two corresponding static solutions are ($U_n\sim k_n^{-1/3}$ and $U_n\sim k_n^{-1}$), leading to spectral properties analogous to what is found in the usual 2D turbulence. The energy spectrum is indeed made of two power laws: $k^{-5/3}$ at wave numbers smaller than the forcing, corresponding to the inverse energy cascade; at larger wave number a power law close to $k^{-3}$, corresponding to the enstrophy cascade.

This type of shell model was considered by Gledzer [11]. Later, Frick [16] considered a modified version of this model which includes also the nonlocal interactions ($U_nU_{n+1}U_{n-j}$, $j=1,2,\ldots$ and corresponding terms). This modified model was used recently by Frick and Aurell to study the direct cascade of enstrophy [17]. In contrast with direct numerical simulations of 2D turbulence which predict steeper spectra than $k^{-3}$ [1], the shell model does not lead to strong deviations from the $k^{-3}$ law. In the shell model, the deviations from the $k^{-3}$ laws are small but systematically increasing with the wave number and are neither consistent with logarithmic [18,19] nor stretched exponential corrections. We shall quantify this discrepancy in Sec. III.

(4) $\varepsilon=2$; in that case $\alpha=0$: [Kolmogorov 1941 (K41) model] and the only conserved quantity is the energy. The fixed point of the shell models is only the Kolmogorov solution $U_n\sim k_n^{-1/3}$.

(5) $\varepsilon=3$; in that case $\alpha=1$ and $\mathrm{sgn}(\varepsilon-1)=1$: The second conserved quantity is the dimensional quadratic equivalent of the "action" [20], a hidden integral of motion in 3D turbulence written in Clebsch variables.

### C. Numerical implementation

Numerical solutions of Eqs. (1) were obtained with $0.2\le\varepsilon\le10.0$. The number of shells used in the simulations was typically of the order of 31 ($0\le n\le30$). The largest number of shells used in the case $\varepsilon=1.25$ was 51($-20\le n\le30$). The value of viscosity $\nu$ was adjusted in the interval $10^{-18}\le\nu\le10^{-8}$ to get in each case the largest possible "inertial" range. The system was forced by random force in zeroth and first shells so that the energy of these shells remains constant ($\rho_0$ and $\rho_1$ are constant, and their phases are random).

The time integration has been done using the fourth-order Runge-Kutta method with fixed time step. The typical time step was $10^{-5}$ except when $\varepsilon=\frac{5}{4}$. In this case, the characteristic times are scale independent, as in 2D turbulence, and an increase of the total number of shells can be made without decreasing the time step. We therefore choose a value of 0.01.

In shell models, each scale is described by only one mode, without reference to any spatial distribution. Therefore statistics can only be obtained as time-averaged characteristics. The (time) averaging is denoted by $\langle\ \rangle$ throughout the rest of this paper. Runs up to $10^8$ time steps were made.

The main characteristics of the models are summarized in Table I: the viscosity, the mean value of the exponent of the third structure function and the relative exponent for the second structure function, the mean energy flux in the "inertial" range, and the two scaling parameters $\Delta$ and $\beta$, defined in Sec. III.

The table includes four cases for $\varepsilon<1$: one corresponding to stable solutions, $\varepsilon=0.33$, one near the onset of the chaotic solution, $\varepsilon=0.39$, one corresponding to the usual GOY model, $\varepsilon=0.5$, and one with $\varepsilon=0.75$. All other data span the range $\varepsilon>1$. Note that in the case $\varepsilon=1$, no energy cascade is present and so the results are very sensitive to initial conditions. We have therefore excluded this pathological case.

We have done some additional simulations for different $\varepsilon<1$ (see Figs. 6–10) but the runs were relatively short and enable only the evaluations of parameters $\Delta$, $\beta$ and not of structure function exponents.

## III. SCALING PROPERTIES OF SHELL MODELS

### A. The She-Lévêque intermittency model

One famous manifestation of scale invariance (3) in turbulence is the self-similarity of the structure functions of the velocity increments over a distance $l$, $\delta v_l=v(x+l)-v(x)$ in the inertial range:

$$\langle\delta v_l^p\rangle=C_p l^{\zeta_p}\quad\text{for all } p\ , \tag{8}$$

where $C_p$ are some numerical constants and $\zeta_p$ some scaling exponents. This property may also be written in a more symmetrical form:

$$\langle\delta v_l^p\rangle=C_{p,s}\langle\delta v_l^s\rangle^{\zeta_p/\zeta_s}\quad\text{for all } p,s\ , \tag{9}$$

where $C_{p,s}$ are some numerical constants and $l$ is in the inertial range. In fact, Benzi *et al.* [21] showed that in 3D isotropic turbulence the property (9) extends over a much larger range of scale, from the injection scale down to a few Kolmogorov scale. It was therefore called extended self-similarity (hereafter ESS). Since then, the

TABLE I. Main characteristics of the shell models studied in this paper: coefficient of the nonlinear terms $\epsilon$, viscosity $\nu$, third order structure function exponent $\zeta_3$, second order structure function relative exponent $\tilde{\zeta}_2$, mean energy dissipation $\langle \epsilon_l \rangle$, intermittency exponent $\Delta$, and hierarchy constant $\beta$.

| $\epsilon$ | $\nu$ | $\zeta_3$ | $\tilde{\zeta}_2$ | $\langle \epsilon_l \rangle$ | $\Delta$ | $\beta$ |
|---|---|---|---|---|---|---|
| 0.33 | $10^{-12}$ | 1.01 | 0.66 | $5.7\times10^{-4}$ | 0.0007±0.0001 | 0.97±0.06 |
| 0.39 | $10^{-12}$ | 1.01 | 0.66 | $4.0\times10^{-5}$ | 0.0020±0.0003 | 0.85±0.10 |
| 0.5 | $2\times10^{-10}$ | 1.03 | 0.72 | $5.8\times10^{-6}$ | 0.45±0.07 | 0.47±0.15 |
| 0.75 | $10^{-9}$ | 1.05 | 0.79 | $1.4\times10^{10^{-5}}$ | 0.65±0.07 | 0.31±0.15 |
| 1.0 | | | | | | |
| 1.15 | $10^{-18}$ | 4.05 | 0.666 | $<10^{-20}$ | −0.013±0.010 | 0.84±0.10 |
| 1.25 | $10^{-18}$ | 3.16 | 0.667 | $\sim10^{-18}$ | 0.013±0.005 | 0.87±0.10 |
| 1.5 | $10^{-14}$ | 2.12 | 0.670 | $\sim10^{-11}$ | 0.077±0.006 | 0.68±0.10 |
| 1.75 | $10^{-13}$ | 1.49 | 0.675 | $3\times10^{-9}$ | 0.13±0.02 | 0.70±0.08 |
| 2.0 | $10^{-13}$ | 1.29 | 0.676 | $8\times10^{-8}$ | 0.18±0.02 | 0.63±0.07 |
| 2.5 | $10^{-12}$ | 1.17 | 0.680 | $1.0\times10^{-6}$ | 0.29±0.02 | 0.59±0.07 |
| 3.0 | $10^{-12}$ | 1.08 | 0.682 | $1.3\times10^{-5}$ | 0.32±0.03 | 0.60±0.07 |
| 4.0 | $10^{-12}$ | 1.03 | 0.689 | $2.6\times10^{-6}$ | 0.29±0.03 | 0.57±0.09 |
| 5.0 | $10^{-12}$ | 1.01 | 0.686 | $5.7\times10^{-6}$ | 0.30±0.04 | 0.54±0.07 |
| 6.0 | $3\times10^{-12}$ | 1.02 | 0.689 | $1.4\times10^{-5}$ | 0.29±0.03 | 0.55±0.08 |
| 7.0 | $10^{-11}$ | 1.0 | 0.69 | $3.6\times10^{-5}$ | 0.28±0.03 | 0.58±0.10 |
| 8.0 | $2\times10^{-10}$ | 1.0 | 0.71 | $8.0\times10^{-5}$ | 0.28±0.03 | 0.55±0.10 |
| 10.0 | $10^{-9}$ | 1.0 | 0.71 | $2.4\times10^{-4}$ | 0.30±0.05 | 0.52±0.10 |

same property was also found in 2D turbulence [22] or in magnetohydrodynamics (MHD) turbulence [23]. This may indicate that it is somehow related to the scale invariance of these systems. As we shall see, this property will also be found in the GOY shell models. In any case, ESS enables better accuracy in the determination of the scaling exponents $\zeta_p$ by enlarging the self-similar range. We shall therefore check and try it on shell models.

The She-Lévêque model [3] predicts a simple shape for the scaling exponents $\zeta_p$. It was later recast by Dubrulle [4] to take into account ESS. The corresponding model then relies on three main hypotheses, involving a dimensionless flux of energy at scale $l$:

$$\pi_l = \frac{\epsilon_l}{\epsilon_l^{(\infty)}} , \tag{10}$$

where $\epsilon_l$ is the mean energy dissipation in a domain of size $l$, and $\epsilon_l^{(\infty)}$ is a normalization function, which enables us to factor out all the geometry dependence of the dissipation. That way, $\pi_l$ truly represents an "inertial range" quantity, independent of external conditions.

The three hypotheses follow.

(i) Similarity:

$$\frac{\delta v_l^3}{\langle \delta v_l^3 \rangle} \overset{\text{scal}}{=} \frac{\epsilon_l}{\langle \epsilon_l \rangle} = \frac{\pi_l}{\langle \pi_l \rangle} , \tag{11}$$

where $\overset{\text{scal}}{=}$ means having the same scaling properties, i.e., that the moments of the corresponding distribution are everywhere proportional, up to a (moment-dependent) numerical constant. This assumption is a natural extension of the Kolmogorov refined similarity hypothesis [24]. Hypothesis (11) is interesting because, contrarily to the Kolmogorov refined similarity hypothesis, it cannot be derived by Taylor's hypothesis, which links the time scale of energy dissipation with the velocity and length scales (see, e.g., the discussion in [7]). Taylor's hypothesis is only meaningful in cases where small eddies are swept by large ones. In shell models, there is no coupling between the large scale velocity and the small scale (the interactions are local in scale space), so that one cannot directly use the Kolmogorov refined similarity hypothesis [7]. Hypothesis (11) is then an interesting alternative. Other solutions may also be found using the multifractal approach [7].

(ii) Moment hierarchy:

$$\frac{\langle \pi_l^{p+1} \rangle}{\langle \pi_l^p \rangle} = A_p \left[ \frac{\langle \pi_l^p \rangle}{\langle \pi_l^{p-1} \rangle} \right]^\beta , \quad 0 \le \beta \le 1 \tag{12}$$

where $A_p$ are numerical constants. Note that the condition $\beta \le 1$ guarantees the convergence of high order moments. The parameter $\beta$ can be interpreted as an anomalous exponent, characterizing the intermittency of the interactions [4]. For example, if the moments follow a power law $\langle \pi_l^p \rangle \sim l^{p\alpha}$ as in Kolmogorov local theory, then $\beta = 1$. In fully developed isotropic 3D turbulence, $\beta = \frac{2}{3}$ [3]. It is not yet clear how $\beta$ depends on the characteristics of the system (conservation laws, boundary conditions, number of degrees of freedom, codimension of the dissipative structures. Giving clues to answer this question is one of the main goals of the present contribution. The interpretation of the constants $A_p$ is also interesting. They mainly depend on the boundary conditions and geometry of the flow [3]. Once they are given, the probability distribution for the interactions is uniquely defined via (12). For example, if $A_p = A_1 = cte$, the interactions follow a $\log_\beta$ Poisson statistics [4,5]. Note also that it means that $\epsilon_l^{(\infty)} \sim \langle \pi_l \rangle^{-\beta^p} \langle \epsilon_l^{p+1} \rangle / \langle \epsilon_l^p \rangle$ for all $p$, so that if $\beta < 1$ we have exactly

$$\varepsilon_l^{(\infty)} \sim \lim_{p\to\infty} \frac{\langle \varepsilon_l^{p+1}\rangle}{\langle \varepsilon_l^{p}\rangle} \ . \tag{13}$$

The normalization factor $\varepsilon_l^{(\infty)}$ can then be interpreted as tracing the tail of the distribution of energy dissipation, i.e., it represents the energy dissipation in the most intermittent structures.

(iii) Power-law intermittency:

$$\langle \pi_l \rangle \sim \left[ \frac{\langle \delta v_l^3 \rangle}{\varepsilon_0 \eta} \right]^{\Delta} , \tag{14}$$

where $\eta$ is the Kolmogorov scale. This assumption merely states that the dissipative structures are spatially intermittent [4].

The combination of the three assumptions ensures that the structure functions follow the extended self-similarity:

$$\langle \delta v_l^p \rangle = C_p \langle \delta v_l^3 \rangle^{\tilde{\zeta}_p} , \tag{15}$$

with a relative exponent:

$$\tilde{\zeta}_p = (1-\Delta)\frac{p}{3} + \Delta \frac{(1-\beta^{p/3})}{(1-\beta)} \ . \tag{16}$$

The scaling of the structure functions in the inertial range $\langle \delta v_l^p \rangle \sim l^{\zeta_p}$ corresponds then simply to an absolute scaling exponent:

$$\zeta_p = \zeta_3 \tilde{\zeta}_p \ . \tag{17}$$

Taking $\zeta_3 = 1$, and $\Delta = \beta = \frac{2}{3}$, one finds the formula proposed by She and Lévêque [3], which fits very well the experimental data on fully developed isotropic 3D turbulence. As we shall see, the GOY class of shell models is characterized by different constants.

### B. Spectra and flux

The spectra are plotted in Fig. 1 for $1.25 \le \varepsilon < 10$. The slope of the spectra can be inferred from the mean value of the second structure function exponent, whose relative value $\tilde{\zeta}_2$ is computed in all cases for $10 \le n \le 20$. All the other characteristics (the energy flux, the relative exponents, the parameters $\Delta$ and $\beta$) were obtained in the same range. They are all given in Table I.

When $\varepsilon = 1.25$ the spectral energy distribution is close to a Kraichnan spectra $E(k) \sim k^{-3}$ with small but systematic deviations, increasing with $n$ [17]. When $\varepsilon$ increases the slope of the spectrum decreases (see Fig. 1). For $\varepsilon = 2$, it is close to $-\frac{5}{3}$ and approaches asymptotically Kolmogorov's law for larger values of $\varepsilon$. At the same time, the average flux of energy increases and energetic bursts produce a spreading of the spectrum towards smallest shells. To remain in the same range of wave numbers (shells) the value of the viscosity has to be increased. The characteristic time needed to obtain accurate mean values of increments also increases. Computational cost limited our simulations to $10^8$ time steps, which is too small to get accurate values for $\tilde{\zeta}_p$ for $\varepsilon > 6$, $p > 4$.

The transport processes (both of energy and of generalized enstrophy) are governed by the triple correlations $\Theta_n$ (2) or by the averaged value $\Phi = \langle \sin(\phi_{n-1} + \phi_n + \phi_{n+1}) \rangle$. The graph of this quantity is given in Fig. 2. It indicates quite different behavior for small and large $\varepsilon$, without noticeable transition at $\varepsilon = 1$. Note that the crossing between negative and positive values occurs at the 2D case $\varepsilon = \frac{5}{4}$. This could explain the quasiequilibrium behavior of the 2D shell model [25].

### C. Structure functions

The velocity structure functions of order $p$ are defined in our shell models as

$$S_p(n) = \langle |U_n|^p \rangle = \langle \rho_n^p \rangle \ , \tag{18}$$

where, as in (2), $\rho_n$ is the modulus of the (complex) velocity. Their scaling properties can be investigated in two ways: either by considering their variation with the wave number $k_n$ ("classical scaling") or using the concept of extended self-similarity (see Sec. III A). In the first case, one looks for a range of wave number in which

$$S_p(n) \sim k_n^{-\zeta_p} \ , \tag{19}$$

where $\zeta_p$ is a local scaling exponent. In the second case, one uses the third structure function as a reference, and one computes the relative scaling exponent $\tilde{\zeta}_p$:

$$S_p(n) \sim \langle \rho_n^3 \rangle^{\tilde{\zeta}_p} \ . \tag{20}$$

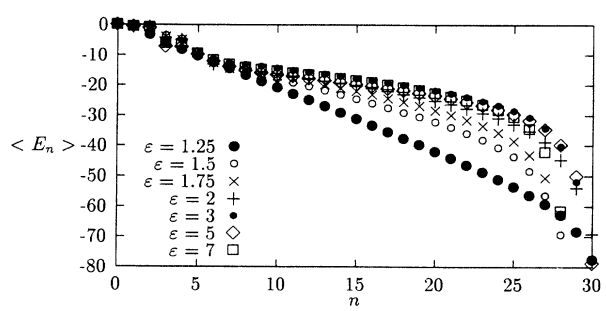


FIG. 1. Energy distribution in the shells.

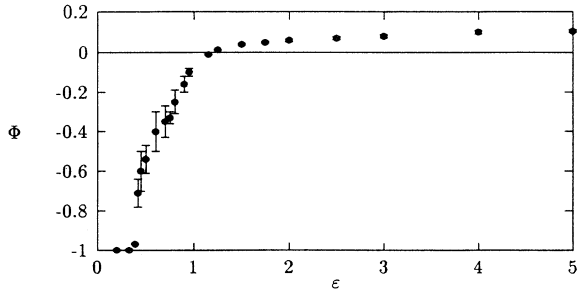


FIG. 2. $\Phi = \langle \sin(\phi_{n-1} + \phi_n + \phi_{n+1}) \rangle$ versus $\varepsilon$.

If ESS also exists in shell models, one expects (20) to hold over a wider range of scale than (19) and to provide a more accurate estimate for the scaling exponents.

This expectation was indeed fulfilled in all cases considered. The most impressive results are given by models in which the spectrum contains very different parts [e.g., increasing, equidistributed, inertial, and dissipative range—see Fig. 3(a) corresponding to $\epsilon=\frac{5}{4}$]. The figure shows the stationary distribution of shell energy in the system with the forcing in the zeroth shell and the output of energy in the largest scale. This kind of spectra obtained in Fig. 3(a) has been obtained by Aurell *et al.* [25], who undertook an investigation of the inverse cascade in shell models. They discovered that the formerly reported inverse $k^{-5/3}$ cascade [11,16] develops only during some transitional stage, being later replaced by a $k^{-1}$ spectrum corresponding to energy equidistribution over the shells. The $k^{-3}$ spectrum (for $n>0$) coincides with the dimensional predictions on the power spectra from a supposed forward cascade of enstrophy, but is well described as a formal statistical equilibrium with enstrophy equidistribution over the shells [25]. Note that in this case, the characteristic time scale is scale independent [$E(k)\sim k^{-3}$; $U_n\sim 2^{-n}$, so that an extended range of shells $-20<n<30$ could be considered].

While a different local scaling exponent would be observed in each corresponding range of scales, a *single* relative scaling exponent suffices to describe the variety of behavior. This is shown in Fig. 3(b), for the second and sixth structure functions. When the logarithms of $S_2$ and $S_6$ are plotted versus the logarithm of $S_3$, beautiful straight lines are obtained. The points corresponding to the positive (inertial and dissipative range) and the negative (increasing and equidistributed range) shell numbers are plotted with different markers. Note that all the points are lying near the same lines.

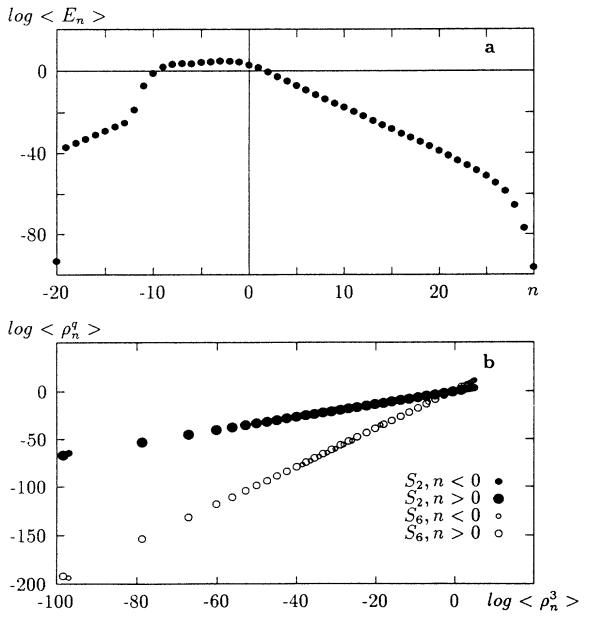


FIG. 3. (a) Energy distribution in the shells. (b) Structure functions $S_2$ and $S_6$ versus $S_3$ in log-log coordinates. The base of the logarithms is 10.

This observation shows that it is more interesting and more reliable to work with relative scaling exponents $\tilde{\zeta}_p$ rather than absolute ones, $\zeta_p$. In the case considered in Fig. 4 ($\epsilon=\frac{5}{4}$), the absolute scaling exponent varies continuously as one goes from the increasing to the dissipative range [see Fig. 4(a)]. It is then difficult to estimate (or even define) accurately the exponent $\zeta_p$. In contrast, the relative scaling exponent may be defined and computed over a much wider range of scales [Fig. 4(b)]. This is another indication that they are the relevant quantities to consider in scale invariant systems. We therefore only focused on the computation of the relative exponents. Their values, up to the sixth order, are given in Table II, as a function of $\epsilon$. Note that the "local" linear K41 prediction $\tilde{\zeta}_p=p/3$ is realized only for models with $\epsilon<0.39$, where $K41$ is a fixed point solution. In all other cases, intermittency is observed with noticeable deviations from the linear law.

### D. Similarity hypothesis

As in fully developed turbulence, the extended self-similarity can be taken into account by a similarity hy-

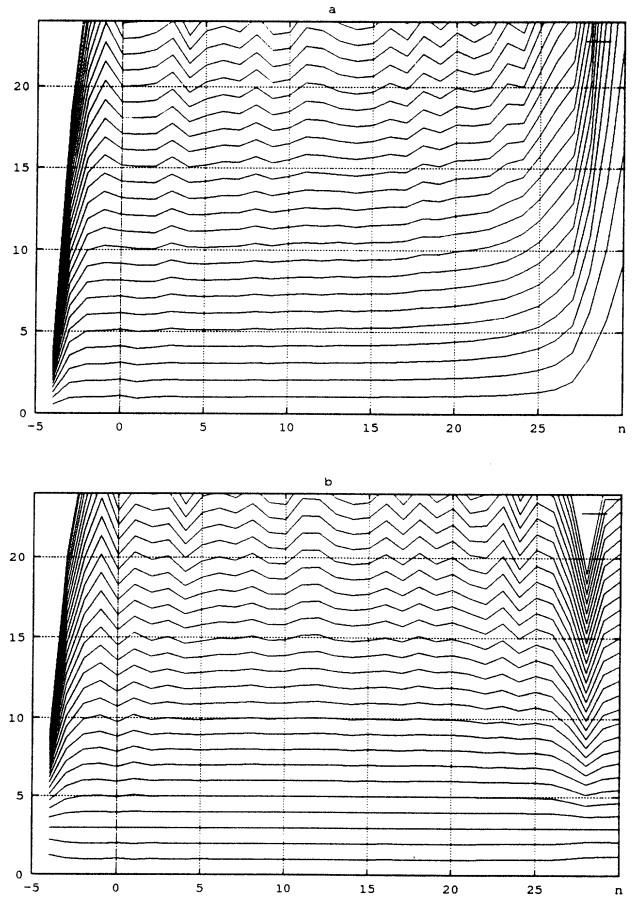


FIG. 4. The scaling exponents $\zeta_p$ (a) and $\tilde{\zeta}_p$ (b) for $\epsilon=1.25$.

TABLE II. Measured relative scaling exponents using extended self-similarity.

| $\varepsilon$ | $\tilde{\zeta}_1$ | $\tilde{\zeta}_2$ | $\tilde{\zeta}_4$ | $\tilde{\zeta}_5$ | $\tilde{\zeta}_6$ |
|---|---|---|---|---|---|
| 0.33 | 0.33 | 0.66 | 1.33 | 1.66 | 2.00 |
| 0.39 | 0.33 | 0.66 | 1.33 | 1.66 | 2.00 |
| 0.5 | 0.40 | 0.71 | 1.27 | 1.53 | 1.81 |
| 0.75 | 0.45 | 0.79 | 1.16 | 1.31 | 1.45 |
| 1.0 | | | | | |
| 1.15 | 0.332 | 0.666 | 1.334 | 1.667 | 2.001 |
| 1.25 | 0.334 | 0.667 | 1.333 | 1.665 | 1.996 |
| 1.5 | 0.337 | 0.670 | 1.327 | 1.652 | 1.975 |
| 1.75 | 0.342 | 0.675 | 1.319 | 1.634 | 1.945 |
| 2.0 | 0.343 | 0.676 | 1.316 | 1.625 | 1.927 |
| 2.5 | 0.346 | 0.680 | 1.307 | 1.601 | 1.885 |
| 3.0 | 0.349 | 0.682 | 1.304 | 1.596 | 1.876 |
| 4.0 | 0.357 | 0.689 | 1.293 | 1.572 | 1.840 |
| 5.0 | 0.355 | 0.686 | 1.296 | 1.574 | 1.851 |
| 6.0 | 0.356 | 0.689 | 1.293 | 1.572 | 1.841 |
| 7.0 | 0.36 | 0.69 | 1.29 | 1.57 | 1.84 |
| 8.0 | 0.38 | 0.71 | 1.28 | 1.55 | 1.82 |
| 10.0 | 0.38 | 0.71 | 1.28 | 1.55 | 1.81 |

pothesis in the spirit of (11). In the case of shell models, it would correspond to

$$\frac{\rho_n^3}{\langle \rho_n^3 \rangle} \overset{\text{scal}}{=} \frac{|\Pi_n|}{\langle |\Pi_n| \rangle} \overset{\text{scal}}{=} \frac{|\Theta_n|}{\langle |\Theta_n| \rangle} , \tag{21}$$

where $\Pi_n$ is the energy flux defined in (2). Taking absolute values is required by the observation that $\rho_n$ is a positive quantity, while $\Pi_n$, which represents a flux, can take negative values. Checking this similarity hypothesis completely would require the evaluation and comparison of the probability distribution functions of $\rho/\langle\rho\rangle$ and $|\Pi|/\langle|\Pi|\rangle$ for each model. To lower the computational cost, we adopted a simplified procedure and compared only some statistical indicators, such as the flatness $\langle\rho^4\rangle/\langle\rho^2\rangle^2$ and the asymmetry $\langle\rho^3\rangle/\langle\rho^2\rangle^{3/2}$. The result is displayed in Fig. 5 for the flatness, and in Fig. 6 for the asymmetry. The result is consistent with the similarity hypothesis. Indeed, the flatness and asymmetry of $\rho$ and $|\Pi|$ follow the same scaling behavior, and differ only by a (scale-independent) constant. In contrast, $\rho$ and $\Pi$ appear to follow different statistics, except in the case $\varepsilon=0.5$ where $\Pi$ and $|\Pi|$ coincide. This result is not really surprising, since $\Pi$ can take negative values while $\rho$ is always positive. The coincidence of statistics for $\Pi$ and $|\Pi|$, however, could not have been anticipated. It is reminiscent of fully developed turbulence, where it was found that both $(\delta v)^3$ and $|(\delta v)^3|$ follow the same scaling behavior [21].

This provides a direct (albeit partial) check of the validity of the similarity hypothesis. Note that a complete (albeit indirect) check of this hypothesis is furnished by the very existence of extended self-similarity.

### E. Moments hierarchy: $\beta$

To check the moments hierarchy (12) hypothesis, we define the nondimensional energy transfer $\pi_n$ as

$$\pi_n \equiv \frac{|\Pi_n|}{\Pi_\infty} , \tag{22}$$

where $\Pi_\infty$ is obtained via [see remark (13)]

$$\Pi_\infty \equiv \lim_{p\to\infty} \frac{\langle |\Pi^{p+1}| \rangle}{\langle |\Pi^p| \rangle} . \tag{23}$$

In practice, $\Pi_\infty$ was evaluated by computing the ratio $\langle|\Pi_{p+1}|\rangle/\langle|\Pi^p|\rangle$ for increasing values of $p$ until some sort of asymptotic limit was obtained (typically for $p\sim 10$). Note that lack of statistics prevents reliable evaluations of the moments of $|\Pi|$ for $p>15$, so that we cannot improve our estimate of $\Pi_\infty$. This procedure probably induces a bias in the subsequent estimate of $\beta$. However, as long as we consider only the lowest order moments, this bias can be expected to be small.

Once the normalization factor $\Pi_\infty$ has been obtained, we may check the hierarchy assumption by plotting the logarithm of $\langle\pi^{p+1}\rangle/\langle\pi^p\rangle$ as a function of the logarithm of $\langle\pi^p\rangle/\langle\pi^{p-1}\rangle$ at different wave numbers $k_n$ and

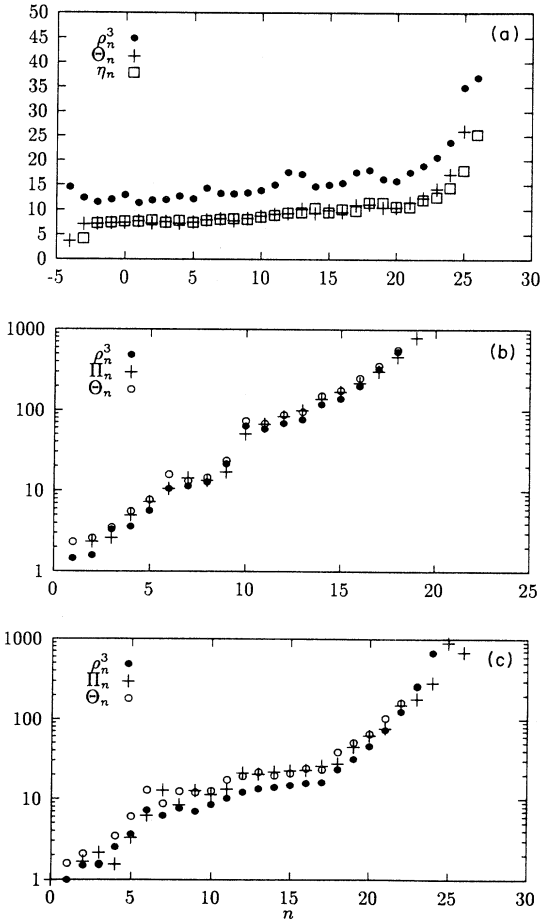


FIG. 5. Flatness factor $\langle x^4\rangle/\langle x^2\rangle^2$ for $\rho_n^3$, $|\Theta_n|$, and $\Theta_n$, $|\Pi_n|$, and $\Pi_n$ (or $|\eta_n|$ and $\eta_n$). (a) $\varepsilon=1.25$; (b) $\varepsilon=0.5$; (c) $\varepsilon=3.0$.

for different $p$. If the moments hierarchy holds, we should obtain a graph made of parallel straight segments: each segment of line corresponds to the hierarchy for a given $p$, at different wave numbers, each segment corresponds to a different $p$. If the hierarchy holds, all segments are characterized by the same slope, $\beta$, but a different origin intercept, $A_p$. If all the segments lie on the same line, then all $A_p$ are equal and the probability distribution of $\pi$ is logarithmic Poisson [4]. Depending on the value of $\varepsilon$, we obtained two types of results. In the "good case," the hierarchy is well established; low order moments are sufficiently separated (in scale) to obtain a good fit to $\beta$. In the "bad case," the segments are very short; it is difficult to define a local slope. However, using a zooming, it is possible to get a rough estimate of $\beta$. Typically, "good cases" are obtained for $\varepsilon > 0.39$ (Fig. 7), while bad cases are obtained for $\varepsilon \leq 0.39$. It is, however, interesting to note that in all the bad cases, $\beta$ measured by zooming was found close to unity.

Another difficulty arises as one approaches the value $\varepsilon = \frac{5}{4}$. In that case, the energy flux tends to zero, and the estimate of the hierarchy becomes very imprecise. In that case, we have checked that the precision can be improved by using the enstrophy flux instead of the energy flux. This flux can be defined in a way analogous to the energy flux as

$$Q_n = k_n^3 \left[ \frac{4\varepsilon - 1}{64} \Theta_{n-1} - \frac{1}{8} \Theta_n \right] . \tag{24}$$

But, in spite of the absence of mean energy flux the evaluations done for energy and enstrophy flux confirm the hierarchy and give the same value of $\beta$.

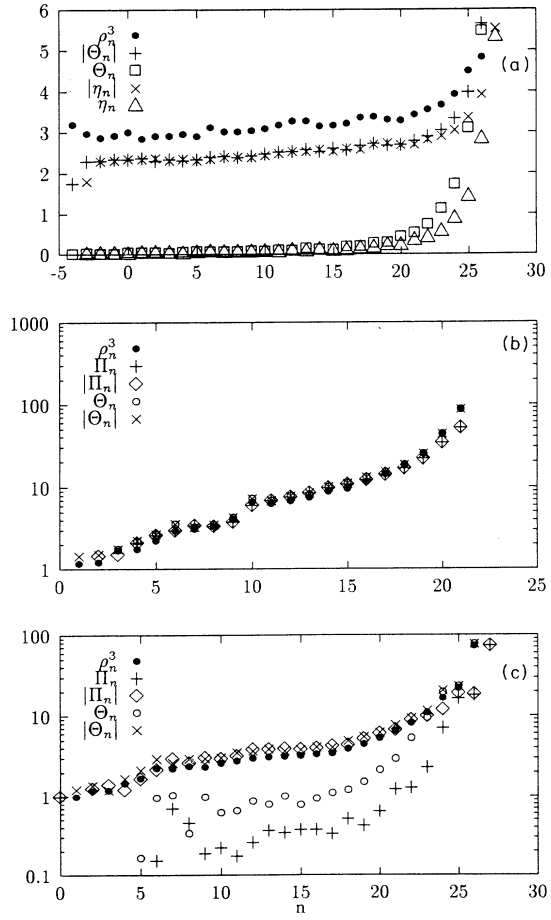


FIG. 6. Asymmetry $\langle x^3 \rangle / \langle x^2 \rangle^{3/2}$ for $\rho_n^3$, $|\Theta_n|$, and $\Theta_n$, $|\Pi_n|$, and $\Pi_n$ (or $|\eta_n|$ and $\eta_n$). (a) $\varepsilon = 1.25$; (b) $\varepsilon = 0.5$; (c) $\varepsilon = 3.0$

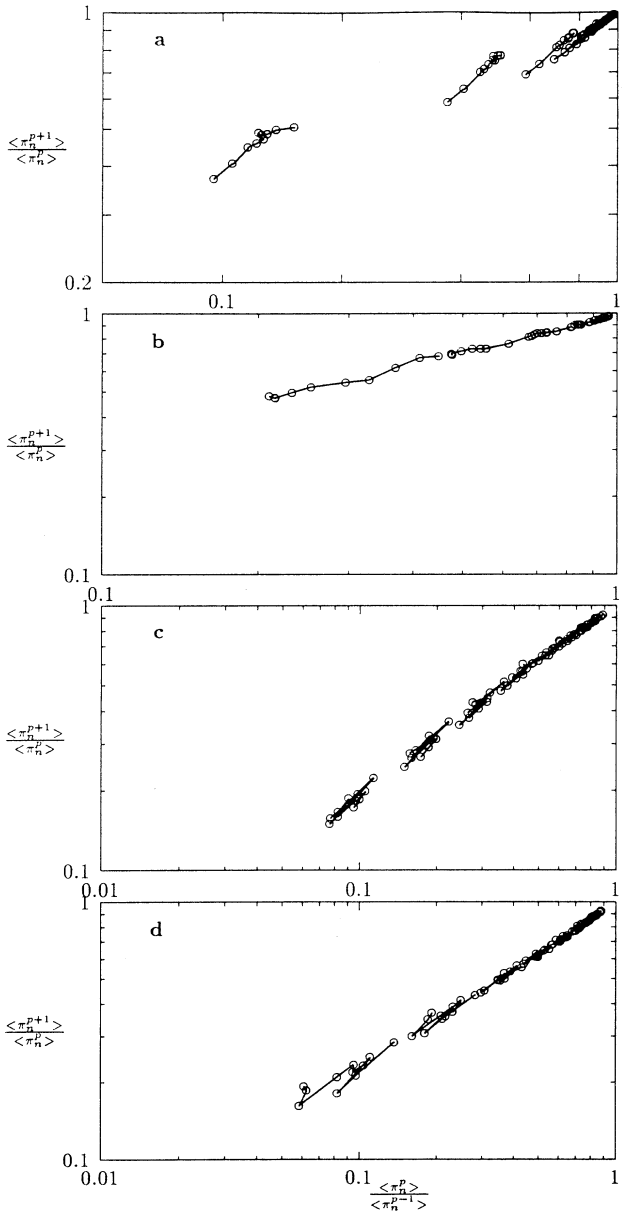


FIG. 7. Definition of $\beta$: (a) $\varepsilon = 0.42$; (b) $\varepsilon = 0.7$; (c) $\varepsilon = 1.25$; (d) $\varepsilon = 3.0$. The points corresponding to the same order ($p$) are connected by lines.

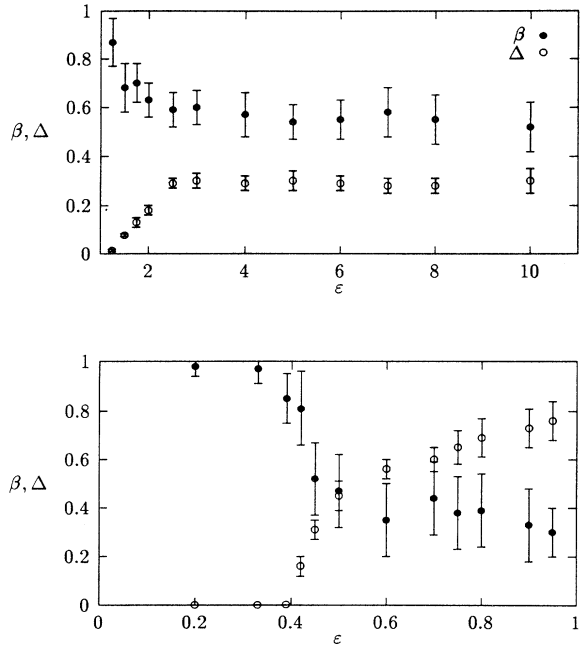


FIG. 8. $\beta$ and $\Delta$ vs $\varepsilon$.

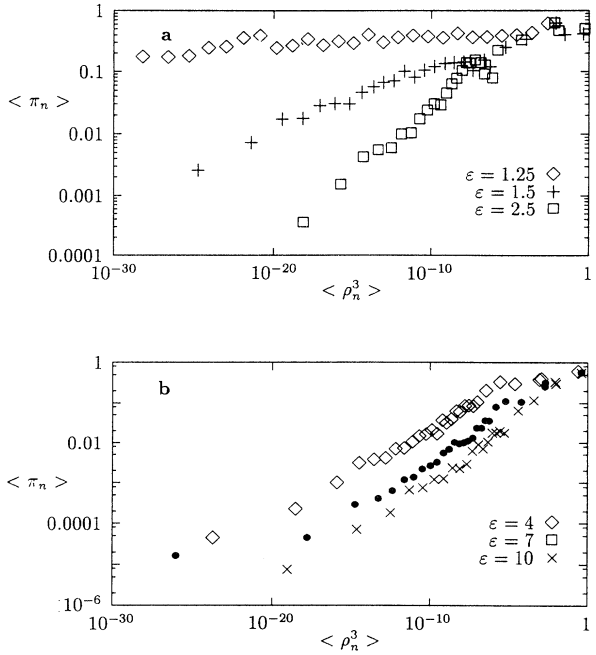


FIG. 9. Definition of $\Delta$: (a) $-1.25 \le \varepsilon \le 2.5$; (b) $-4 \le \varepsilon \le 10$.

All the values of $\beta$ as a function of $\varepsilon$ are given in Fig. 8 and Table I. For clarity, the range $0 < \varepsilon < 1$ has been enlarged. Note the steady decrease of $\beta$ between 1 and 0 for $\varepsilon > 1$ and the crossing occurring at $\varepsilon = 0.39$, where $\beta$ goes from values $\sim 1$ to values $< 1$. Note also the discontinuity appearing at $\varepsilon = 1$, which seems to indicate that systems with $\varepsilon < 1$ or $\varepsilon > 1$ belong to a distinct scaling class.

TABLE III. Theoretical relative scaling exponents obtained using formula (16) and the values of $\Delta$ and $\beta$ measured. The error in the scaling exponent is $\pm 0.01$ in all cases.

| $\varepsilon$ | $\Delta$ | $\beta$ | $\zeta_1$ | $\zeta_2$ | $\zeta_4$ | $\zeta_5$ | $\zeta_6$ |
|---|---|---|---|---|---|---|---|
| 0.33 | 0.0007 | 0.97 | 0.33 | 0.67 | 1.33 | 1.67 | 2.00 |
| 0.39 | 0.002 | 0.85 | 0.33 | 0.67 | 1.33 | 1.67 | 2.00 |
| 0.5 | 0.45 | 0.47 | 0.37 | 0.70 | 1.27 | 1.52 | 1.76 |
| 0.75 | 0.65 | 0.31 | 0.42 | 0.74 | 1.21 | 1.39 | 1.55 |
| 1.0 | | | | | | | |
| 1.15 | −0.013 | 0.84 | 0.33 | 0.67 | 1.33 | 1.67 | 2.00 |
| 1.25 | 0.013 | 0.87 | 0.33 | 0.67 | 1.33 | 1.67 | 2.00 |
| 1.5 | 0.077 | 0.68 | 0.34 | 0.67 | 1.33 | 1.65 | 1.98 |
| 1.75 | 0.13 | 0.70 | 0.34 | 0.67 | 1.32 | 1.64 | 1.96 |
| 2.0 | 0.18 | 0.63 | 0.34 | 0.68 | 1.32 | 1.63 | 1.93 |
| 2.5 | 0.29 | 0.59 | 0.35 | 0.68 | 1.30 | 1.60 | 1.88 |
| 3.0 | 0.32 | 0.60 | 0.35 | 0.68 | 1.30 | 1.59 | 1.87 |
| 4.0 | 0.29 | 0.57 | 0.35 | 0.68 | 1.30 | 1.59 | 1.86 |
| 5.0 | 0.30 | 0.54 | 0.35 | 0.68 | 1.30 | 1.59 | 1.87 |
| 6.0 | 0.29 | 0.55 | 0.35 | 0.69 | 1.30 | 1.59 | 1.87 |
| 7.0 | 0.28 | 0.58 | 0.35 | 0.68 | 1.30 | 1.60 | 1.88 |
| 8.0 | 0.28 | 0.55 | 0.35 | 0.68 | 1.30 | 1.59 | 1.87 |
| 10.0 | 0.30 | 0.52 | 0.36 | 0.69 | 1.30 | 1.58 | 1.86 |

### F. Intermittency: $\Delta$

Our estimate of $\Pi_\infty$ can also be used to check the intermittency hypothesis (14) and to compute the intermittency parameter $\Delta$. In our shell models, it is obtained via

$$\langle \pi_n \rangle = \frac{\langle |\Pi_n| \rangle}{\Pi_\infty} \sim \langle \rho_n^3 \rangle^\Delta . \tag{25}$$

The curves $\langle \Pi_n \rangle$ vs $\langle \rho_n^3 \rangle$ are displayed in Fig. 9 for $1 < \varepsilon < 10$. The corresponding intermittency parameter as a function of $\varepsilon$ can be found in Table I and in Fig. 8. One may note that the behavior of $\Delta$ as a function of $\varepsilon$ is similar to the behavior of the mean flux parameter $\Phi$ for $\varepsilon > 1$ and similar to $\Phi + 1$ for $\varepsilon < 1$ (Fig. 2). As for $\beta$, $\Delta$ is characterized by two distinct features: a crossing between $\Delta = 0$ and $\Delta \neq 0$ occurring at $\varepsilon = 0.39$, and a discontinuity appearing at $\varepsilon = 1$.

### G. Probability distribution functions

We have seen that the constants in the hierarchy are independent of the order of the hierarchy for $\varepsilon > 2$ and for $0.5 \le \varepsilon < 1$. This means that the logarithmic Poisson statistics for the energy transfer, discussed in [4,5], is only achieved for these $\varepsilon$. In Fig. 10 we show the probability distribution function for $\log_{10}\pi$ measured in our shell models for $\varepsilon = 0.42$ ("non-Poisson case") and $\varepsilon = 3$ (logarithmic Poisson case) at a scale inside the "inertial range." Both distributions are strongly skewed towards negative $\log_{10}\pi$ and display an exponential wing, as in 3D turbulence. The dotted line shows the comparison with a logarithmic Poisson distribution:

$$P(Y)=\frac{\lambda^Y e^{-\lambda}}{\Gamma(Y+1)}, \quad -1<Y<\infty \tag{26}$$

with $Y=\log_\beta(\pi C)$. The $\lambda$ was chosen to ensure that $\langle Y\rangle=(\langle\log_{10}\pi\rangle+C)/\log_{10}\beta$; $C$ is a constant related to the $A_p$ in the hierarchy [Eq. (12)], which determines the position of the cutoff on the right side of the maximum. The fits shown use $\lambda=15.6$ and $C=3300$ for $\varepsilon=0.42$ and $\lambda=8.8$ and $C=329$ for $\varepsilon=3$, together with $\beta=0.6$ and 0.55 as measured from the moment hierarchy. As may be seen from Fig. 10, the fit is rather good for $\varepsilon=3$ and rather poor (except at the origin) for $\varepsilon=0.42$.

## IV. DISCUSSION

In this paper, we have studied a general class of shell models, focusing on their scaling properties. This class of models covers a wide variety of dynamical properties, characterized by a parameter $\varepsilon$. For $\varepsilon<0.39$, the models have a stable fixed point solution, corresponding to K41 solution. Shell models with $\varepsilon>0.39$ have a chaotic dynamics. The shell models are characterized by two conservation laws, the energy and a generalized enstrophy.

We have checked that the property of extended self-similarity is common to all the models studied, thereby providing further evidence that this property is common to many scale invariant systems. Using the extended self-similarity, we have measured the scaling exponents $\zeta_p$ of the velocity structure functions up to order 6. Their relative value, $\zeta_p/\zeta_3$, is provided in Table II. Deviations from the linear K41 law are observed, whenever the system crosses the value $\varepsilon=0.39$.

Our next result concerns the existence of the moment hierarchy (12), which is observed in 3D isotropic turbulence [8]. This hierarchy is clearly observed in models with $\varepsilon>0.39$, with measurable $\beta$ and $\Delta$ parameters (Figs. 7–9). The constants of the hierarchy, $A_p$, seem to approach a constant value only for $\varepsilon>2$. Therefore proba-

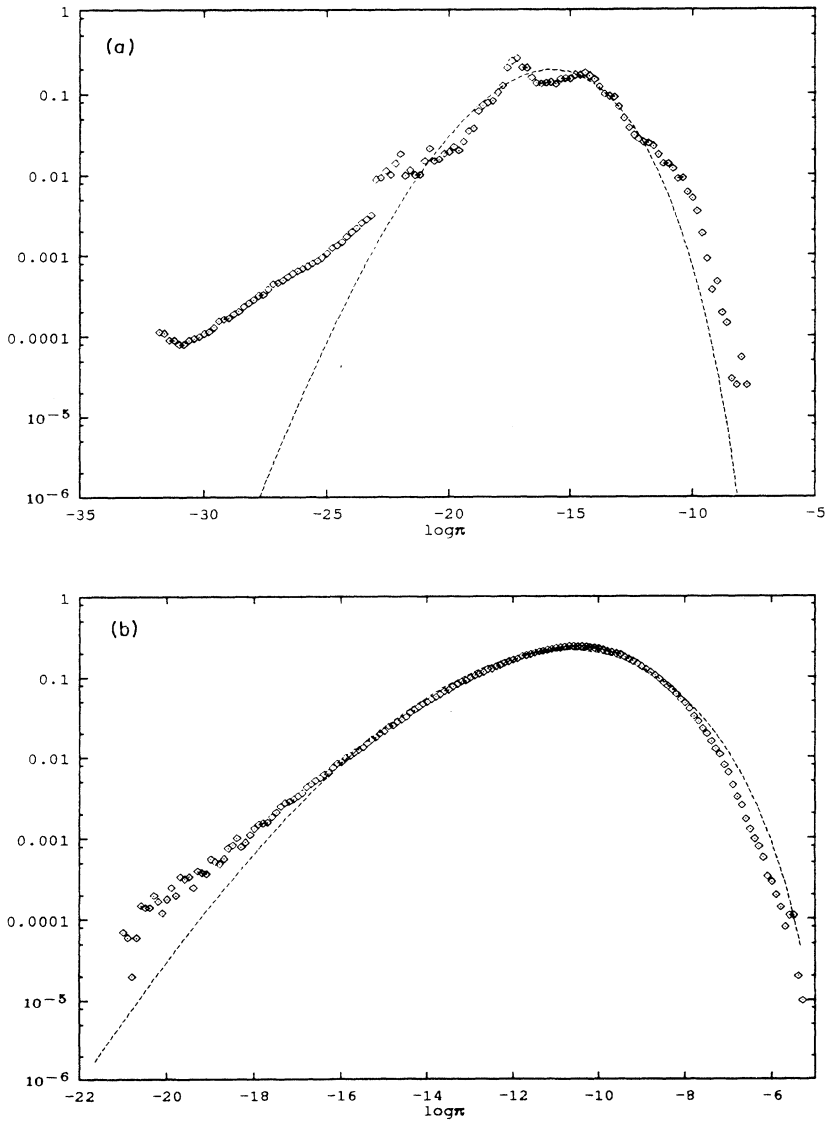


FIG. 10. Probability distribution function of energy flux $|\Pi|$: (a) $\varepsilon=0.42$, (b) $\varepsilon=3.0$. The base of the logarithms is 10.

bility distributions for the energy transfer are exactly logarithmic Poisson only in the cases $\varepsilon > 2$. This was confirmed by direct measurements of the probability distribution function. However, even in the case $\varepsilon < 2$, the measured probability distribution functions display exponential wings and nonzero skewnesses, features also observed in 3D turbulence. This might be an indication that they are a signature of the moment hierarchy, and are characteristic of this class of systems. To check that the hierarchy is responsible with the intermittency in the scaling exponents, we have computed the "theoretical" relative scaling exponents, given by Eq. (16), using the values of $\beta$ and $\Delta$ measured directly. The result is given in Table III. Comparison with the measured values given in Table III shows that the best agreement (less than 1%) is obtained for $1 < \varepsilon < 4$ and $\varepsilon < 0.39$. The deterioration of the agreement observed for large values of $\varepsilon$ could be linked with the deterioration of the statistics, due to computational limitations. An interesting observation is that the agreement between the universal relation (16) and the measured scaling exponents can be improved (up to 1% level) for slightly lower values of $\beta$, which are shown in Fig. 11. For $\varepsilon > 1$, these "best values" follow a scaling relation

$$\beta_{\text{best}} = \left[ \frac{\varepsilon - \varepsilon_1}{\varepsilon_1} \right]^{-\gamma}, \tag{27}$$

with $\varepsilon_1 = 0.3843$ and the critical exponent $\gamma = 0.4$. A similar scaling law seems to hold for $0.39 < \varepsilon < 1$, with a different normalization (about four times smaller), but with the same critical exponent ( see Fig. 11).

If we accept the idea that, at least for $\varepsilon > 1$, our class of shell models satisfies the moment hierarchy also observed in 3D turbulence, we now have at our disposal a unique set of data about this hierarchy as a function of the properties of the system. Figure 8 summarizes our results and shows $\beta$ and $\Delta$ as a function of $\varepsilon$. Clearly, even in systems with similar characteristics, variation of these two parameters can be observed, although a sort of saturation towards $\Delta = 0.3$ seems to occur at large $\varepsilon$. This shows that neither $\Delta$ nor $\beta$ can be regarded as universal quantities and seem to depend on the system. This is a little bit disappointing, because it removes hopes to find a simple method to compute these parameters in each system. We may, however, note that the case $\varepsilon = 1$, characterizing the

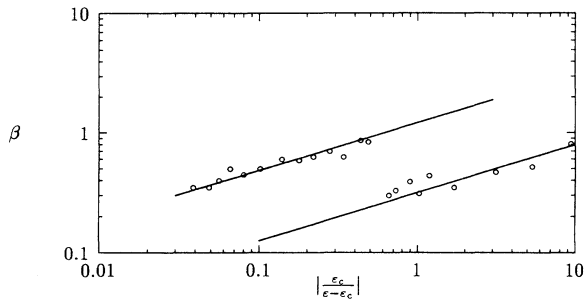


FIG. 11. $\beta$ versus $\varepsilon_1/(\varepsilon - \varepsilon_1)$ in log-log coordinates. The lines correspond to power laws with exponent 0.4.

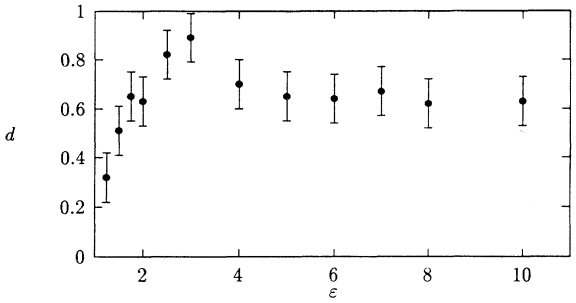


FIG. 12. Codimension of dissipative structures $d = \Delta/(1-\beta)$ versus $\varepsilon$.

transition between systems with helicitylike ($\varepsilon < 1$) or enstrophylike ($\varepsilon > 1$) conservation laws, clearly corresponds to some transition, since both $\beta$ and $\Delta$ are discontinuous there. This indicates that the conservation laws play a non-negligible role in the determination of these two parameters. For the sake of completeness, we also computed the codimension of dissipation structures, defined as $d = \Delta/(1-\beta)$ (see, e.g., [3]) in the case $\varepsilon > 1$ (see Fig. 12). In fully 3D developed turbulence, where the dissipative structures are filaments, this codimension is of the order of 2 [3]. In the present case, it increases from 0.2 for $\varepsilon = 1.25$ up to 0.9 for $\varepsilon = 3$ and settles down to 0.6 for larger $\varepsilon$. Again, this parameter does not appear to be "universal."

In summary, we have shown that shell models present the same kind of scaling properties as 3D turbulence, but with different parameters depending on the conservation laws. This confirms and extends a recent work by Benzi *et al.* [7], who showed that only shell models conserving the energy and the helicity display the same intermittency as in 3D turbulence. It is clear that additional theoretical work is needed to understand some results obtained in this paper. For example, we have not tried to investigate the influence of the viscosity on the scaling properties. Preliminary studies indicate that it may play a role [7]. Also, it would be interesting to use more realistic models of turbulence to study the nonlocal scale invariance. We are currently investigating the scale invariance properties of "tree-shell models" [26] (in which more than one shell is used to describe one scale) along the lines followed in this paper.

## ACKNOWLEDGMENTS

This work was supported by a grant from the European Community (Grant No. ERBCHRXCT920001), the French Government Program "Relance de l'Est," and Groupement de Recherche CNRS-IFREMER "Mécanique des Fluides Géophysiques et Astrophysiques." One of us (P.F.) acknowledges partial support from the Russian Foundation of Fundamental Investigation (Grant No. 94-01-00951-a).

[1] A. Babiano, C. Basdevant, B. Legras, and R. Sadourny, J. Fluid Mech. **183**, 379 (1987).
[2] V. Borue, Phys. Rev. Lett. **72**, 1475 (1994).
[3] Z.-S. She and E. Lévêque, Phys. Rev. Lett. **72**, 336 (1994).
[4] B. Dubrulle, Phys. Rev. Lett. **73**, 959 (1994).
[5] Z.-S. She and E. C. Waymire, Phys. Rev. Lett. **74**, 262 (1995).
[6] L. Biferale, A. Lambert, R. Lima, and G. Paladin, Physica D **80**, 105 (1995).
[7] L. Kadanoff, D. Lohse, J. Wang, and R. Benzi, Phys. Fluids **7**, 617 (1995).
[8] G. Ruiz-Chavarria, C. Baudet, and S. Ciliberto, Phys. Rev. Lett. **74**, 1986 (1995).
[9] V. Desnjansky and E. Novikov, Prikl. Mat. Mekh. **38**, 507 (1974).
[10] M. Yamada and K. Ohkitani, J. Phys. Soc. Jpn. **56**, 4210 (1987).
[11] E. B. Gledzer, Sov. Phys. Dokl. **18**, 216 (1973).
[12] M. H. Jensen, G. Paladin, and A. Vulpiani, Phys. Rev. A **43**, 798 (1991).
[13] D. Pisarenko, L. Biferale, D. Courvoisier, U. Frisch, and M. Vergassola, Phys. Fluids A **5**, 2533 (1993).
[14] R. Benzi, L. Biferale, and G. Parisi, Physica D **65**, 163 (1993).
[15] L. Biferale (private communication).
[16] P. Frick, Magnetohydrodynamics (USSR) **19**, 48 (1983).
[17] P. Frick and E. Aurell, Europhys. Lett. **24**, 725 (1993).
[18] R. H. Kraichnan, J. Fluid Mech. **47**, 525 (1971).
[19] G. Falkovich and V. Lebedev, Phys. Rev. E **49**, R1800 (1994).
[20] V. Yakhot and V. Zakharov, Physica D **64**, 379 (1993).
[21] R. Benzi, S. Ciliberto, C. Baudet, G. Ruiz, and R. Tripiccione, Europhys. Lett. **24**, 275 (1993).
[22] A. Babiano, B. Dubrulle, and P. Frick (unpublished).
[23] V. Carbone, Phys. Rev. E **50**, R671 (1994).
[24] A. N. Kolmogorov, J. Fluid Mech. **13**, 82 (1962).
[25] E. Aurell, G. Boffetta, A. Crisanti, P. Frick, G. Paladin, and A. Vulpiano, Phys. Rev. E **50**, 4705 (1994).
[26] E. Aurell, P. Frick, and V. Shaidurov, Physica D **72**, 95 (1994).